
DETAILMASTER: Can Your Text-to-Image Model Handle Long Prompts?

Qirui Jiao^{1*}, Daoyuan Chen^{2*}, Yilun Huang², Xika Lin³, Ying Shen¹, Yaliang Li²
¹Sun Yat-Sen University, ²Alibaba Group, ³Worcester Polytechnic Institute

Abstract

While recent text-to-image (T2I) models show impressive capabilities in synthesizing images from brief descriptions, their performance significantly degrades when confronted with long, detail-intensive prompts required in professional applications. We present **DETAILMASTER**, the first comprehensive benchmark specifically designed to evaluate T2I models' systematical abilities to handle extended textual inputs that contain complex compositional requirements. Our benchmark introduces four critical evaluation dimensions: Character Attributes, Structured Character Locations, Multi-Dimensional Scene Attributes, and Explicit Spatial/Interactive Relationships. The benchmark comprises long and detail-rich prompts averaging 284.89 tokens, with high quality validated by expert annotators. Evaluation on 7 general-purpose and 5 long-prompt-optimized T2I models reveals critical performance limitations: state-of-the-art models achieve merely $\sim 50\%$ accuracy in key dimensions like attribute binding and spatial reasoning, while all models showing progressive performance degradation as prompt length increases. Our analysis highlights systemic failures in structural comprehension and detail overload handling, motivating future research into architectures with enhanced compositional reasoning. We open-source the dataset, data curation code, and evaluation tools to advance detail-rich T2I generation and enable broad applications that would otherwise be infeasible due to the lack of a dedicated benchmark.

1 Introduction

Recently, text-to-image (T2I) generation has experienced remarkable development, achieving higher-quality image synthesis and expanding practical products [5, 11, 21, 32]. However, while text-conditioned control offers a convenient way to generate desired images, most current models are primarily optimized for short textual inputs. They often struggle with long and complex prompts (see Figure 1 and Appendix J for failure cases), which may consist of hundreds of tokens and contain rich details (e.g., character attributes, spatial relationships, and diverse scene properties).

The limitations of text-to-image models in faithfully following long prompts can be attributed to four constraints: 1) **Training data bias**. The mainstream models are primarily trained on short prompts (e.g., COCO [25] averaging 10.5 tokens, CC12M [7] averaging 20.2 tokens), reinforcing a bias toward concise textual inputs. 2) **Structural comprehension deficiency**. Most text encoders show limitations in parsing hierarchical descriptions involving multiple objects, attributes, and their spatial relationships. They may incorrectly segment information and fall into attribute misalignment. 3) **Detail overload**. When prompts contain excessive descriptive details about a single subject, models tend to omit or distort specific characteristics. 4) **Token length constraints**. Most text encoders impose strict upper bounds on input tokens (e.g., CLIP's 77-token limit [34]).

*Equal contribution.

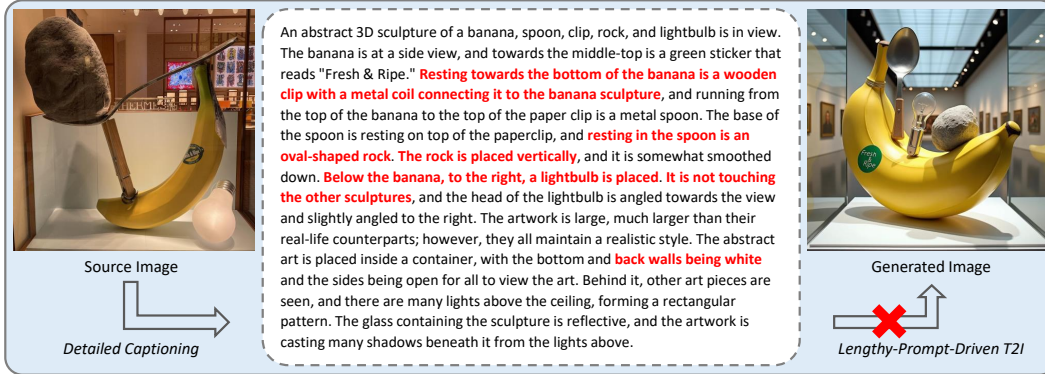


Figure 1: Text-to-image errors in long prompt scenario (with FLUX.1-dev). Real source image (left), detailed caption/prompt (center), and generated image (right). Red text indicates failure points.

The ability to faithfully adhere to long prompts is crucial in many practical scenarios where users have extensive requirements. Developing a robust benchmark for evaluating long-prompt-driven image generation is of significant research and practical value, across domains like interactive media, visual storytelling, scientific visualization, industrial prototyping, and so on [6, 20, 46, 49]. Existing evaluations of text-to-image models have examined their capabilities across multiple dimensions, including image-text alignment, attribute binding, spatial relationships, and human preference. However, these evaluations predominantly rely on short prompts. A few existing benchmarks involve long-prompt scenarios [17, 28], but they remain limited by constrained token lengths (typically around 100 tokens) and lack detailed attribute descriptions and scene context.

To facilitate a more rigorous evaluation of text-to-image models in long-prompt scenarios, we introduce **DETAILMASTER**, a novel benchmark along with a robust evaluation protocol. Our benchmark is constructed based on four critical dimensions of prompt comprehension and adherence: 1) **Character Attributes**, 2) **Structured Character Locations**, 3) **Multi-Dimensional Scene Attributes**, and 4) **Explicit Spatial or Interactive Relationships**. The prompts in our benchmark are derived from existing detailed captioning data [30, 33], which we further refine by augmenting missing visual details, resulting in an average token length of 284.89. To ensure high quality, human experts are engaged to evaluate our benchmark, confirming its high standard. Regarding the evaluation protocol, we develop specialized assessment mechanisms for each category of attributes, enabling systematic evaluation of models' compositional T2I abilities in long-prompt scenarios.

Employing the **DETAILMASTER** benchmark, we investigate 7 general-purpose models, including state-of-the-art (SOTA) models FLUX [21] and GPT Image-1 [31], along with 5 specialized models optimized for long prompts. The experimental results and analysis provide valuable insights into the critical limitations of current text-to-image techniques in handling detail-rich long prompts. For example, even the most advanced models achieve merely $\sim 50\%$ accuracy in generating correct character-level features in such scenario. Furthermore, the optimized models' performance is heavily constrained by their backbone architectures. And there is a consistent degradation in prompt adherence as prompt length increases, highlighting fundamental challenges in handling long prompts.

In summary, our contributions are three-fold: (1) We propose the **DETAILMASTER** benchmark, with a comprehensive evaluation dataset and a robust evaluation protocol to systematically assess T2I models' prompt comprehension and adherence in long-prompt scenarios; (2) We conduct extensive comparisons on both popular text-to-image models and those specifically optimized for long prompts with **DETAILMASTER**, deriving rich insights for further improvements; (3) We open-source all data and code (<https://github.com/modelscope/data-juicer/tree/DetailMaster>) to facilitate future research in text-to-image generation for long, detail-rich prompts.

2 Related works

Text-to-image models. Text-to-image generation aims to synthesize semantically aligned images conditioned on textual descriptions. Initial endeavors predominantly use Generative Adversarial Net-

Table 1: Comparison of data composition between **DETAILMASTER** and other benchmarks. Detailed statistical analysis provided in Section 5.1.

Benchmark	# Prompts	# Nouns	Character		# Scene Attributes	# Entity Relationships	Avg. Tokens
			# Attributes	# Locations			
HRS-Comp [4]	3004	620	1000	N/A	N/A	2000	16.43
T2I-CompBench [19]	6000	2316	4000	N/A	N/A	2000	12.65
DensePrompts [28]	7061	4913	N/A	N/A	N/A	N/A	100.04
DPG-Bench [17]	1065	4286	5020	N/A	329	2593	83.91
DETAILMASTER (Ours)	4116	5165	37165	6910	12330	18526	284.89

works (GANs) [13], such as StackGAN [53] and AttnGAN [50], employing a generator-discriminator framework to produce images. Subsequent advancements introduce autoregressive models that treat image generation as a sequence prediction task. Models like DALL-E [37] and Parti [52] employ transformer architectures to generate image tokens sequentially, conditioned on textual prompts. More recently, diffusion-based models [16] have emerged as a powerful paradigm. These models, including DALL-E 2 [36], Imagen [39], and Stable Diffusion [38], operate by iteratively denoising random noise to produce coherent images. Beyond this, flow-based models such as Stable Diffusion 3.5 [11] and FLUX [21] use flow matching [26] techniques to learn direct transformations from noise to images, reducing sampling complexity and improving efficiency. Furthermore, the proprietary models Gemini 2.0 Flash [14] and GPT Image-1 [31] also show SOTA level performance.

Benchmarks for text-to-image generation. Early evaluations for text-to-image generation primarily use datasets such as CUB Birds [43] and Oxford Flowers [29], which have limited diversity and simple prompts. Recently, benchmarks like DrawBench [39], PartiPrompts [52], HRS-Bench [4] and T2I-CompBench [19] introduce diverse sets of prompts aimed at evaluating compositional generation abilities, including object presence, attribute binding, and spatial relationships. To precisely measure the alignment between generated images and every detail within the prompts, benchmarks such as TIFA [18] and Gecko [45] decompose prompts into elemental components and generate corresponding questions to assess model fidelity. Moreover, benchmarks like GenAI-Bench [22], RichHF18K [24] and HPS v2 [48] involve human annotators to rank image-text pairs, aiming to train preference-aligned evaluators that reflect human judgment. However, these benchmarks predominantly focus on short prompts. They overlook the long and complex prompts, which can significantly affect the generation with intricate elements and details, such as increasing the risk of attribute misalignment.

Text-to-image models for long prompt. To enhance text-to-image models’ ability to follow long prompts, some studies employ large language models (LLMs) as text encoders to improve semantic extraction. Representative models such as Imagen [39], DeepFloyd IF [3], and advanced approaches like Stable Diffusion 3.5 [11] and FLUX [21] adopt frozen T5 [35] as their text encoder, strengthening text-image alignment. Beyond this, ParaDiffusion [47] uses a frozen Llama V2 [42] as its text encoder and constructs a training dataset for long prompts to enhance comprehension. LLM4GEN [28] introduces an adapter to fuse features from multiple text encoders (e.g., T5 and CLIP) and proposes a specialized loss to penalize attribute mismatch. ELLA [17] incorporates a trainable mapper after the LLM-based text encoder to improve information extraction from long prompts. LongAlign [27] decomposes long prompts into individual sentences for separate encoding, while also enabling preference optimization for long-text alignment. LLM Blueprint [12] extracts object details from long prompts using an LLM, then employs layout-to-image generation and an iterative refinement scheme for image synthesis. However, due to the scarcity of benchmarks for long-prompt-driven image generation, these methods lack fair comparison. Thus, we propose the **DETAILMASTER** benchmark to systematically assess their performance.

Benchmarks for long-prompt-driven text-to-image generation. Current benchmarks for long-prompt-driven image generation remain scarce. DensePrompts [28] collects 100 detailed web images, using GPT-4V [1] to generate attribute-rich descriptions and expand the length. DPG-Bench [17] aggregates multi-short-prompt annotations from existing datasets and employs GPT-4 [2] to synthesize them into long descriptions. However, these benchmarks exhibit critical limitations: 1) oversimplified evaluation, relying on CLIP Score [15] for text-image alignment or binary feature verification via multimodal large language model (MLLMs), which fails to assess fine-grained and compositional accuracy; 2) constrained prompt length and details, deriving prompts through coarse LLM extraction

and failing to match real-world long-prompt complexity. To address these issues, we propose **DETAILMASTER**, a novel benchmark featuring longer prompts along with a fine-grained evaluation protocol to rigorously assess text-to-image generation under complex long-prompt scenarios. As evidenced in Table 1, our benchmark advances prior works through extended prompts, enlarged attribute sets, and more comprehensive evaluation objectives.

3 The DETAILMASTER Benchmark

3.1 Dataset construction

3.1.1 Overview

To better simulate the challenges in long-prompt scenarios, our dataset requires prompts of sufficient length and rich details. Hence, we leverage existing human-annotated detailed captioning datasets, where each sample comprises an image paired with fine-grained textual descriptions, including DOCCI (15K samples) [30] and Localized Narratives (Flickr30k [51] and COCO subsets, 149K samples) [33], and expand their captions. While these datasets already provide precise object attribute descriptions with an average token length of 68.4, their coverage is still incomplete. To enhance image description quality and obtain optimal prompts, we design a robust and fine-grained attribute extraction pipeline that systematically captures four categories of key features: 1) **Character Attributes**, where we categorize main characters (objects, animals, persons, and others) and analyze them via class-specific attribute extraction protocols; 2) **Structured Character Locations**, where we employ a nine grid-based spatial partitioning scheme to assign precise positions; 3) **Multi-Dimensional Scene Attributes**, decomposing scenes hierarchically into background, lighting conditions, and stylistic elements; and 4) **Explicit Spatial/Interactive Relationships**, annotating character pairs with geometric (e.g., “dog behind chair”) and dynamic interactions (e.g., “holding”). These extracted attributes are then integrated into the original captions using LLM-based expansion, yielding richly detailed prompts with an average token length of 284.89. Beyond prompt enhancement, they also form the foundation for constructing specialized evaluation metrics. The overview of the data generation process is shown in Figure 2. To enhance reusability, our data construction process is also implemented as data processing operators and configurable data recipes within Data-Juicer [8, 9].

3.1.2 Attribute extraction pipeline

Main character identification. We first need to know what characters are present in each sample. Specifically, we provide an MLLM with both the source image and the original caption to detect main characters within the image. We then apply sample filtering to retain only instances containing more than 4 main characters, ensuring as many high-quality features as possible in the final prompt to better evaluate models’ structural comprehension and their ability to handle detail overload.

Character localization. For character localization, we detect each main character using both an MLLM and the open-set object detector YOLOE-11L [44] to generate two bounding box predictions. We then establish a validation where the two boxes with an Intersection over Union (IoU) score at least 0.7 are considered mutually confirmatory, with the larger one selected as the valid bounding box. For cases with IoU less than 0.7, we crop sub-images of each box and employ BLIP [23] to compute image-text matching scores between each sub-image and the character name. If both scores fall below 0.4, we discard both detections; otherwise, we retain the higher-scoring box. Finally, we transform validated bounding boxes into structured spatial descriptions using the nine-region partitioning scheme detailed in Appendix A. They are recorded as “Structured Character Locations”.

Character attribute extraction. For character attribute extraction, we implement a hierarchical pipeline. Initially, each main character is classified by an LLM into one of four predefined categories: object, animal, person, or other. Subsequently, category-specific instructions are applied to guide the LLM in extracting relevant character attributes from the original captions, such as material and shape for objects, color and movement patterns for animals, and clothing and age for persons, thereby generating preliminary attribute lists. To enhance attribute completeness and simulate detail overload, we then implement a multimodal refinement stage. For characters with valid bounding box information, we extract corresponding sub-images and ask an MLLM to supplement the text-derived

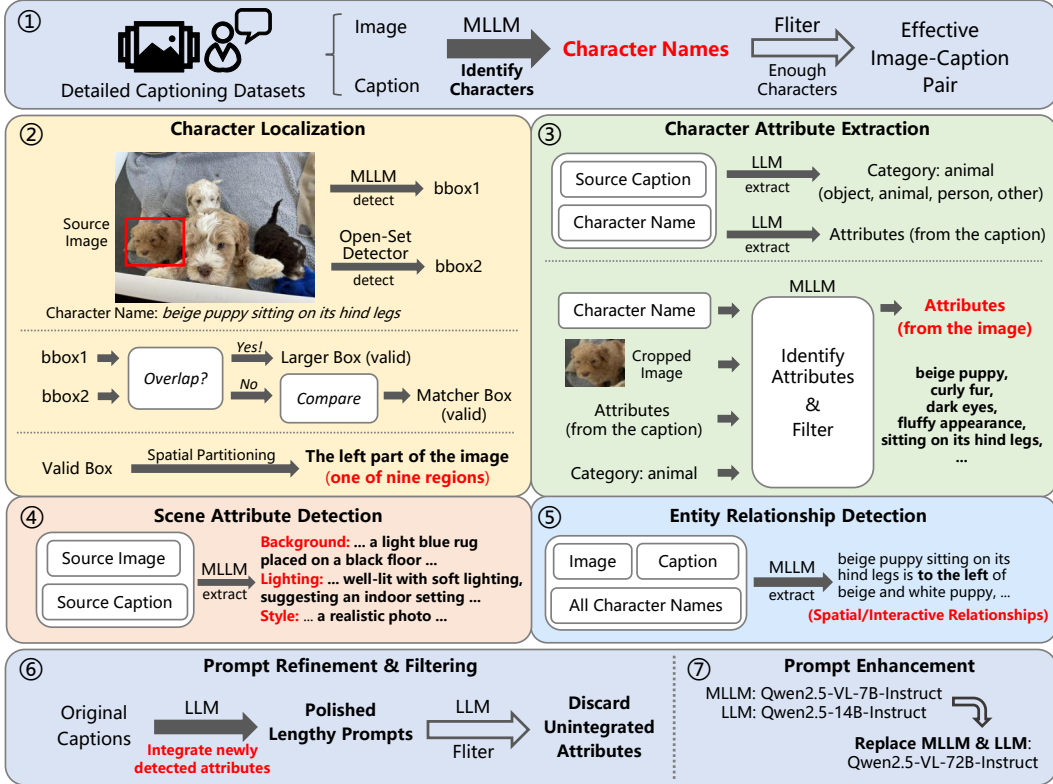


Figure 2: Overview diagram of the data construction process for the **DETAILMASTER** benchmark.

attribute lists with visually-grounded features. The synthesized output from both textual and visual analysis constitutes the final “Character Attributes” for each character.

Scene attribute and entity relationship detection. For scene attributes extraction, we employ an MLLM to jointly analyze both the source image and the original caption, characterizing background composition, lighting conditions, and stylistic elements of each sample. These features are recorded as “Scene Attributes”. Regarding entity relationship extraction, we input each sample’s source image, original caption, and all detected characters, into the MLLM. The model then performs relationship parsing to identify and extract all discernible spatial configurations and interactive relationships between entities, which are finally recorded as “Explicit Spatial/Interactive Relationships.”

3.1.3 Prompt refinement & enhancement

Prompt refinement and filtering. Following the attribute extraction, we implement a prompt refinement pipeline to transform the original captions into detail-rich long prompts. For each sample, we enumerate all identified main characters and employ an LLM to incorporate both “Character Attributes” and “Structured Character Locations” of each character into the original caption. Subsequently, the same LLM integrates the sample’s “Scene Attributes” and “Explicit Spatial/Interactive Relationships” to produce the refined prompt. Beyond prompt refinement, the extracted attributes are ultimately used to generate evaluation metrics. To guarantee the accuracy of evaluation metric, we implement an attribute validation mechanism where an LLM verifies the presence of each attribute in the refined prompt, filtering out any attributes that fail to be incorporated. In addition, samples with less than four valid character-level attributes are filtered out.

Prompt enhancement. Throughout the attribute extraction and prompt refinement pipeline, we employ Qwen2.5-14B-Instruct [40] as our primary LLM and Qwen2.5-VL-7B-Instruct [41] as the MLLM. This initial process yields 4,565 detail-rich prompts, with an average token length of 237.53. To achieve higher precision and greater detail, we subsequently reprocess the corresponding

4,565 samples using Qwen2.5-VL-72B-Instruct as both the LLM and the MLLM. This new process generates an improved dataset containing 4,116 prompts with an average token length of 284.89.

3.2 Evaluation protocol

3.2.1 Overview

Quantitatively measuring the quality of compositional text-to-image generation proves inherently difficult, as it demands fine-grained cross-modal understanding between textual prompts and generated images. Popular approaches typically employ object detection models for spatial verification, vision-language models for image-text alignment [15], and MLLMs for attribute verification [10, 19]. However, these methods often yield coarse-grained evaluations that may introduce noise and compromise measurement accuracy. To address these limitations, we develop a robust multi-stage evaluation pipeline that systematically assesses the accuracy of all four categories of attributes.

3.2.2 Evaluation metrics

Regarding the design of evaluation metrics, we utilize all four categories of attributes that we previously extract. For the “Character Attributes” metric, we count the number of correctly generated attributes for each character, and compute accuracy by dividing the total number of correct attributes by the total attributes of characters per category (categorized as object, animal, or person). The “Character Locations” metric involves tallying the number of correctly positioned characters, with accuracy derived from the ratio of accurately placed characters to all locatable characters. For “Entity Relationships”, we examine each relationship in every sample and calculate the proportion of correct relationships. These three metrics assess attribute mismatches and omissions in detail-rich scenarios. For the “Scene Attributes” metric, we compute accuracy for background, lighting, and style, evaluating overall image fidelity in long prompt scenarios.

In the main text, our evaluations are conducted on the full version of **DETAILMASTER**, comprising 4,116 prompts. Additionally, we design a mini version of our benchmark to facilitate rapid evaluation for researchers, which consists of 800 detail-rich prompts. The details are in Appendix H.

3.2.3 Evaluation pipeline

We design a multi-step evaluation pipeline to systematically assess the performance of text-to-image models. First, we need to instruct the T2I model with the prompts from **DETAILMASTER** to generate corresponding image sets. Next, we detect and localize the characters present in the generated images. Subsequently, we conduct a rigorous quantitative evaluation across four critical dimensions: Character Attributes, Character Locations, Scene Attributes, and Entity Relationships, deriving accuracy rates for each evaluated model. To ensure computational efficiency and resource optimization, we employ Qwen2.5-VL-7B-Instruct as the MLLM throughout the evaluation process. Further details of the evaluation pipeline are provided in Appendix E.

4 Experiments

4.1 Experimental setup

We evaluate the performance of seven general-purpose models and five long-prompt optimized models. Among the general-purpose models, five are open-source implementations including Stable Diffusion 1.5 [38], SD-XL [32], DeepFloyd IF[39], Stable Diffusion 3.5 Large [11], and FLUX.1-dev [21], while two are proprietary commercial systems, specifically the image generation modules of Gemini 2.0 Flash [14] and GPT-4o [31]. The long-prompt optimized models include LLM4GEN [28], ELLA [17], LongAlign [27], LLM Blueprint [12], and ParaDiffusion [47]. Detailed configurations for all the evaluated models are provided in Appendix B. Regarding the evaluation metrics, we assess each model across four key generation tasks: Character Attributes, Character Locations, Scene Attributes, and Entity Relationships, enabling systematic assessment of compositional text-to-image generation in long-prompt scenarios. The results are presented in Table 2.

Table 2: Evaluation results on the **DETAILMASTER** Benchmark. We evaluate model performance across four key tasks: character attributes, character locations, scene attributes, and entity relationships. All values in the table represent accuracy percentages.

(A) General-Purpose Text-to-Image Model									
Model	Backbone	Character Attributes			Character Locations	Scene Attributes			Entity Relationships
		Object	Animal	Person		Background	Light	Style	
SD1.5 [38]	-	20.79	27.69	13.89	8.68	22.02	64.52	80.90	5.88
SD-XL [32]	-	24.41	29.54	16.73	10.95	27.52	68.42	68.87	9.83
DeepFloyd IF [3]	-	31.01	37.47	25.61	14.28	26.26	67.87	86.49	11.95
SD3.5 Large [11]	-	48.56	46.20	32.95	33.62	89.61	90.33	95.69	40.03
FLUX.1-dev [21]	-	51.47	45.83	34.91	41.57	95.77	97.05	94.81	47.49
Gemini 2.0 Flash [14]	-	55.44	47.84	34.23	44.74	96.69	95.90	97.20	50.78
GPT Image-1 [31]	-	59.41	48.04	40.40	53.92	97.50	98.85	97.69	63.07

(B) Long-Prompt Optimized Text-to-Image Model									
Model	Backbone	Character Attributes			Character Locations	Scene Attributes			Entity Relationships
		Object	Animal	Person		Background	Light	Style	
LLM4GEN [28]	SD1.5	21.75	29.14	17.20	9.22	25.60	65.71	50.11	7.44
LLM Blueprint [12]	SD1.5	21.41	27.01	13.91	18.44	50.89	77.57	64.24	11.60
ELLA [17]	SD1.5	34.50	35.14	22.01	15.92	47.12	74.28	40.14	16.64
LongAlign [27]	SD1.5	32.95	34.60	15.35	14.89	77.03	87.70	72.27	19.17
ParaDiffusion [47]	SD-XL	35.25	33.28	22.29	20.32	83.65	92.21	67.45	25.50

4.2 Performance evaluations on **DETAILMASTER**

4.2.1 Comparisons across general-purpose text-to-image models

Impact of token length constraints. As shown in Table 2, models employing CLIP as the text encoder (SD1.5 and SD-XL) show significant limitations when handling long prompts due to token length constraints, consistently underperforming across all four tasks. In contrast, DeepFloyd, which employs T5 as its text encoder, benefits from an extended input capacity and visibly outperforms the former two models. Nevertheless, its performance remains bad, constrained by both the quality of its training data and inherent architectural limitations.

Performance ceiling of SOTA models. SD3.5 and FLUX, which combine T5 with enhanced training data and superior model architecture, show improvements over previous models. These two models achieve remarkable performance on “Scene Attributes”, attaining accuracy exceeding 90%, indicating robust scene control capability. However, their performance remains constrained on the other three tasks, suggesting that the absence of explicit training on long prompts limits their adaptability. The proprietary models, Gemini 2.0 Flash and GPT Image-1, outperform all aforementioned open-source models. Nevertheless, their accuracy for “Character Attributes”, “Character Locations”, and “Entity Relationships” also plateaus at around 50%, indicating that even SOTA models have considerable room for improvement in long prompt scenarios.

4.2.2 Comparisons across long-prompt optimized text-to-image models

Dense prompt training matters more than increasing token capacity. While LLM4GEN uses an adapter to infuse T5 features, its 128-token limit during training fails to address long prompt challenges, leading to slight improvements. ELLA maintains the same constraint but train with dense and complex prompt, yielding more improvements than LLM4GEN. With a similar architecture and training strategy, ParaDiffusion extends the limit to 512 during training, enabling superior performance. Compared to DeepFloyd (with same token capacity but conventional training), ParaDiffusion shows better performance across almost all metrics. These results validate that while expanded token capacity provides necessary infrastructure, dense prompt training yields greater gains.

Decomposition and iteration mitigates long-prompt challenges. LongAlign decomposes long prompts for separate encoding and trains with long prompts, indirectly increasing the token capacity and achieving notable gains. LLM Blueprint identifies key roles and locations from long prompts, followed by iterative image refinement, yielding notable improvements in “Character Locations”.

Table 3: Attribute accuracy of detected generated characters across models.

Character Attributes	SD-XL	DeepFloyd IF	SD3.5 Large	FLUX.1-dev	Gemini 2.0 Flash	GPT Image-1
Object	79.17	81.19	86.55	89.01	90.06	91.77
Animal	84.27	82.73	89.39	90.37	90.37	92.31
Person	80.65	83.35	89.10	91.06	92.46	94.10
Character Attributes	SD1.5	LLM4GEN	LLM Blueprint	ELLA	LongAlign	ParaDiffusion
Object	74.66	75.62	72.01	82.06	82.58	83.22
Animal	80.30	81.46	79.91	84.55	84.87	84.29
Person	75.93	77.90	71.98	84.55	82.48	83.40

Performance bottlenecks in backbone architectures. Nevertheless, current long-prompt optimized methods predominantly build upon SD1.5 and SD-XL. While these methods show measurable improvements over their baseline counterparts, their overall performance remains unsatisfactory.

4.2.3 Analysis on key generation tasks

Task-specific performance trends. Consistent performance trends are shown across generation tasks, with stronger models achieving higher scores. Notably, “Character Attributes”, “Character Locations”, and “Entity Relationships” remain challenging, while “Scene Attributes” proves easier. Interestingly, for the “style” attribute, the optimized models underperform baseline models. This may attribute to the predominance of realistic styles in the dataset: while SD1.5 naturally aligns with real-world styles, optimizations may introduce undesirable deviations.

Stronger models, fewer attribute misalignment and loss. To further analyze model behavior, we calculate attribute accuracy specifically for the detected generated characters (excluding missing ones), revealing how models handle attribute misalignment and omission. As shown in Table 3, advanced or optimized models show superior attribute accuracy for generated characters, indicating their enhanced prompt comprehension and better attribute-character alignment capabilities.

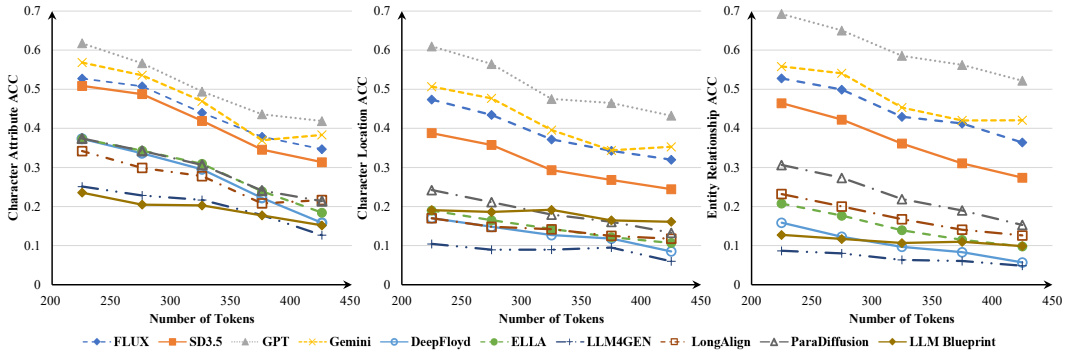


Figure 3: Negative correlation between generation accuracy and prompt token length.

4.3 Negative correlation between prompt length and adherence.

To better understand the impact of prompt length on text-to-image generation, we analyze the relationship between prompt token length (tokenized using CLIP’s tokenizer) and the accuracy of “Character Attributes”, “Character Locations”, and “Entity Relationships”. We employ five distinct length intervals: below 250, above 400, and three 50-token intervals spanning 250-400. The results, illustrated in Figure 3, show a consistent negative correlation between prompt length and generation accuracy across 10 evaluated models (excluding SD1.5 and SD-XL). This indicates that current text-to-image models indeed struggle to faithfully interpret and execute long prompts, suggesting substantial room for improvement in handling complex prompt scenarios.

Furthermore, we conduct additional analysis on the relationship between prompt length and attribute misalignment, visualizing how attribute accuracy for generated characters decreases with longer prompts. The details are shown in Appendix G.

5 Evaluation of data quality and diversity

5.1 Data statistics

We present a statistical analysis of our **DETAILMASTER** Benchmark. The dataset consists of 4,116 prompts, covering 5,165 distinct nouns with an average prompt length of 284.89 tokens. The token length distribution reveals: 285 prompts at 100-200, 2,399 prompts at 200-300, 1,151 prompts at 300-400, and 281 prompts exceed 400. Regarding evaluation metrics: 1) The “Character Attributes” category includes 8,597 valid characters annotated with 37,165 distinct features (comprising 22,728 for “object”, 4,810 for “animal”, and 9,627 for “person”). 2) The “Character Locations” category contains 6,910 character position annotations. 3) For “Scene Attributes”, we annotate 4,104 background descriptions, 4,114 lighting descriptions, and 4,112 style descriptions. 4) The “Entity Relationships” category contains 18,526 explicit spatial/interactive relationship annotations. As illustrated in Table 1, our benchmark surpasses existing benchmarks for compositional or long-prompt-driven image generation through more comprehensive metrics and longer prompts, enabling rigorous assessment of text-to-image models’ capacities in handling complex, long prompts.

5.2 Human evaluation

To assess the data quality of our **DETAILMASTER** Benchmark, we randomly select 50 samples from each evaluation task (400 in total) and employ two expert annotators to evaluate them. The final scores are derived through an averaging process. The human evaluation criteria comprises three primary dimensions: 1) **Task Relevance**. We evaluate whether the evaluation data properly aligns with the designated evaluation tasks. 2) **Source Image Fidelity**. We evaluate whether the evaluation data accurately aligns with the original images from the detailed captioning dataset (for hallucination assessment). 3) **Prompt Consistency**. We evaluate whether the evaluation content is described in the final polished prompts. The results show that 100% of samples meet task relevance requirements, 93.6% maintain visual fidelity with original images, and 97.5% show complete consistency with final polished prompts. These findings validate that the evaluation data of **DETAILMASTER** faithfully derives from authentic image-caption pairs, ensuring its validity. Furthermore, the strong alignment between evaluation data and final prompts mitigates accuracy evaluation errors caused by missing attribute descriptions. These results collectively confirm the high quality and robustness of our benchmark. Detailed human evaluation results for specific sub-tasks are provided in Appendix D.

6 Overview of more experiments and analysis

In Appendix A, we examine our spatial partitioning scheme designed for extracting “Character Locations” features and validate its effectiveness. Appendix B details configurations of all evaluated models. Appendix C documents the resource requirement. Appendix D documents the full human evaluation results, further confirming the high quality of **DETAILMASTER**. Appendix E describes implementation details of our evaluation pipeline. Appendix F verifies the non-sensitive impact of randomness when using LLMs in our evaluation. Appendix G studies the positive correlation between prompt length and attribute misalignment. Appendix H presents the mini version of **DETAILMASTER** along with corresponding results. Appendix I presents detailed discussion of limitations. Appendix J showcases case studies, validating the correctness of our evaluation conclusions.

7 Conclusion

We present **DETAILMASTER**, a benchmark for evaluating text-to-image generation in long prompt scenarios, along with a robust and fine-grained evaluation protocol. Our benchmark comprises 4,116 long and detail-rich prompts, with an average token length of 284.89. The evaluation covers four key generation tasks: “Character Attributes”, “Structured Character Locations”, “Multi-Dimensional Scene Attributes”, and “Explicit Spatial/Interactive Relationships”. And we assess 7 general-purpose and 5 long-prompt-optimized T2I models, comparing their architectural designs and optimization strategies, and derive key insights: generation accuracy declines as prompt length increases, with even SOTA models achieving only ~50% accuracy, indicating substantial room for improvement. We hope our proposed benchmark and evaluation protocol will drive advancements in text-to-image models for long prompts, enabling better adherence to user instructions in specialized domains.

References

- [1] Josh Achiam, Steven Adler, Sandhini Agarwal, Lama Ahmad, Ilge Akkaya, Florencia Leoni Aleman, Diogo Almeida, Janko Altenschmidt, Sam Altman, Shyamal Anadkat, et al. Gpt-4 technical report. *arXiv preprint arXiv:2303.08774*, 2023.
- [2] Josh Achiam, Steven Adler, Sandhini Agarwal, Lama Ahmad, Ilge Akkaya, Florencia Leoni Aleman, Diogo Almeida, Janko Altenschmidt, Sam Altman, Shyamal Anadkat, et al. Gpt-4 technical report. *arXiv preprint arXiv:2303.08774*, 2023.
- [3] DeepFloyd Lab at StabilityAI. DeepFloyd IF: a novel state-of-the-art open-source text-to-image model with a high degree of photorealism and language understanding. <https://www.deepfloyd.ai/deepfloyd-if>, 2023. Retrieved on 2023-11-08.
- [4] Eslam Mohamed Bakr, Pengzhan Sun, Xiaoqian Shen, Faizan Farooq Khan, Li Erran Li, and Mohamed Elhoseiny. Hrs-bench: Holistic, reliable and scalable benchmark for text-to-image models. In *Proceedings of the IEEE/CVF International Conference on Computer Vision*, pages 20041–20053, 2023.
- [5] James Betker, Gabriel Goh, Li Jing, Tim Brooks, Jianfeng Wang, Linjie Li, Long Ouyang, Juntang Zhuang, Joyce Lee, Yufei Guo, et al. Improving image generation with better captions. *Computer Science. https://cdn.openai.com/papers/dall-e-3.pdf*, 2(3):8, 2023.
- [6] Yihan Cao, Siyu Li, Yixin Liu, Zhiling Yan, Yutong Dai, Philip Yu, and Lichao Sun. A survey of ai-generated content (aigc). *ACM Computing Surveys*, 57(5):1–38, 2025.
- [7] Soravit Changpinyo, Piyush Sharma, Nan Ding, and Radu Soricut. Conceptual 12m: Pushing web-scale image-text pre-training to recognize long-tail visual concepts. In *Proceedings of the IEEE/CVF conference on computer vision and pattern recognition*, pages 3558–3568, 2021.
- [8] Daoyuan Chen, Yilun Huang, Zhijian Ma, Heseng Chen, Xuchen Pan, Ce Ge, Dawei Gao, Yuexiang Xie, Zhaoyang Liu, Jinyang Gao, et al. Data-juicer: A one-stop data processing system for large language models. In *Companion of the 2024 International Conference on Management of Data*, pages 120–134, 2024.
- [9] Daoyuan Chen, Haibin Wang, Yilun Huang, Ce Ge, Yaliang Li, Bolin Ding, and Jingren Zhou. Data-juicer sandbox: A feedback-driven suite for multimodal data-model co-development. *arXiv preprint arXiv:2407.11784*, 2024.
- [10] Jaemin Cho, Yushi Hu, Roopal Garg, Peter Anderson, Ranjay Krishna, Jason Baldridge, Mohit Bansal, Jordi Pont-Tuset, and Su Wang. Davidsonian scene graph: Improving reliability in fine-grained evaluation for text-to-image generation. *arXiv preprint arXiv:2310.18235*, 2023.
- [11] Patrick Esser, Sumith Kulal, Andreas Blattmann, Rahim Entezari, Jonas Müller, Harry Saini, Yam Levi, Dominik Lorenz, Axel Sauer, Frederic Boesel, et al. Scaling rectified flow transformers for high-resolution image synthesis. In *Forty-first international conference on machine learning*, 2024.
- [12] Hanan Gani, Shariq Farooq Bhat, Muzammal Naseer, Salman Khan, and Peter Wonka. Llm blueprint: Enabling text-to-image generation with complex and detailed prompts. *arXiv preprint arXiv:2310.10640*, 2023.
- [13] Ian J Goodfellow, Jean Pouget-Abadie, Mehdi Mirza, Bing Xu, David Warde-Farley, Sherjil Ozair, Aaron Courville, and Yoshua Bengio. Generative adversarial nets. *Advances in neural information processing systems*, 27, 2014.
- [14] Google. Gemini 2.0 flash image generation. <https://ai.google.dev/gemini-api/docs/image-generation#gemini>, 2025.
- [15] Jack Hessel, Ari Holtzman, Maxwell Forbes, Ronan Le Bras, and Yejin Choi. Clipscore: A reference-free evaluation metric for image captioning. *arXiv preprint arXiv:2104.08718*, 2021.
- [16] Jonathan Ho, Ajay Jain, and Pieter Abbeel. Denoising diffusion probabilistic models. *Advances in neural information processing systems*, 33:6840–6851, 2020.
- [17] Xiwei Hu, Rui Wang, Yixiao Fang, Bin Fu, Pei Cheng, and Gang Yu. Ella: Equip diffusion models with llm for enhanced semantic alignment. *arXiv preprint arXiv:2403.05135*, 2024.
- [18] Yushi Hu, Benlin Liu, Jungo Kasai, Yizhong Wang, Mari Ostendorf, Ranjay Krishna, and Noah A Smith. Tifa: Accurate and interpretable text-to-image faithfulness evaluation with question answering. In *Proceedings of the IEEE/CVF International Conference on Computer Vision*, pages 20406–20417, 2023.
- [19] Kaiyi Huang, Kaiyue Sun, Enze Xie, Zhenguo Li, and Xihui Liu. T2i-compbench: A comprehensive benchmark for open-world compositional text-to-image generation. *Advances in Neural Information Processing Systems*, 36:78723–78747, 2023.
- [20] Ting-Hao Huang, Francis Ferraro, Nasrin Mostafazadeh, Ishan Misra, Aishwarya Agrawal, Jacob Devlin, Ross Girshick, Xiaodong He, Pushmeet Kohli, Dhruv Batra, et al. Visual storytelling. In *Proceedings of the 2016 conference of the North American chapter of the association for computational linguistics: Human language technologies*, pages 1233–1239, 2016.

- [21] Black Forest Labs. Flux. <https://github.com/black-forest-labs/flux>, 2024.
- [22] Baiqi Li, Zhiqiu Lin, Deepak Pathak, Jiayao Emily Li, Xide Xia, Graham Neubig, Pengchuan Zhang, and Deva Ramanan. Genai-bench: A holistic benchmark for compositional text-to-visual generation. In *Synthetic Data for Computer Vision Workshop@ CVPR 2024*, 2024.
- [23] Junnan Li, Dongxu Li, Caiming Xiong, and Steven Hoi. Blip: Bootstrapping language-image pre-training for unified vision-language understanding and generation. In *International conference on machine learning*, pages 12888–12900. PMLR, 2022.
- [24] Youwei Liang, Junfeng He, Gang Li, Peizhao Li, Arseniy Klimovskiy, Nicholas Carolan, Jiao Sun, Jordi Pont-Tuset, Sarah Young, Feng Yang, et al. Rich human feedback for text-to-image generation. In *Proceedings of the IEEE/CVF Conference on Computer Vision and Pattern Recognition*, pages 19401–19411, 2024.
- [25] Tsung-Yi Lin, Michael Maire, Serge Belongie, James Hays, Pietro Perona, Deva Ramanan, Piotr Dollár, and C Lawrence Zitnick. Microsoft coco: Common objects in context. In *Computer vision—ECCV 2014: 13th European conference, zurich, Switzerland, September 6–12, 2014, proceedings, part v 13*, pages 740–755. Springer, 2014.
- [26] Yaron Lipman, Ricky TQ Chen, Heli Ben-Hamu, Maximilian Nickel, and Matt Le. Flow matching for generative modeling. *arXiv preprint arXiv:2210.02747*, 2022.
- [27] Luping Liu, Chao Du, Tianyu Pang, Zehan Wang, Chongxuan Li, and Dong Xu. Improving long-text alignment for text-to-image diffusion models. *arXiv preprint arXiv:2410.11817*, 2024.
- [28] Mushui Liu, Yuhang Ma, Zhen Yang, Jun Dan, Yunlong Yu, Zeng Zhao, Zhipeng Hu, Bai Liu, and Changjie Fan. Llm4gen: Leveraging semantic representation of llms for text-to-image generation. In *Proceedings of the AAAI Conference on Artificial Intelligence*, volume 39, pages 5523–5531, 2025.
- [29] Maria-Elena Nilsback and Andrew Zisserman. Automated flower classification over a large number of classes. In *2008 Sixth Indian conference on computer vision, graphics & image processing*, pages 722–729. IEEE, 2008.
- [30] Yasumasa Onoe, Sunayana Rane, Zachary Berger, Yonatan Bitton, Jaemin Cho, Roopal Garg, Alexander Ku, Zarana Parekh, Jordi Pont-Tuset, Garrett Tanzer, et al. Docti: Descriptions of connected and contrasting images. In *European Conference on Computer Vision*, pages 291–309. Springer, 2024.
- [31] OpenAI. Gpt image-1. <https://openai.com/index/introducing-4o-image-generation/>, 2025.
- [32] Dustin Podell, Zion English, Kyle Lacey, Andreas Blattmann, Tim Dockhorn, Jonas Müller, Joe Penna, and Robin Rombach. Sdxl: Improving latent diffusion models for high-resolution image synthesis. *arXiv preprint arXiv:2307.01952*, 2023.
- [33] Jordi Pont-Tuset, Jasper Uijlings, Soravit Changpinyo, Radu Soricut, and Vittorio Ferrari. Connecting vision and language with localized narratives. In *Computer Vision—ECCV 2020: 16th European Conference, Glasgow, UK, August 23–28, 2020, Proceedings, Part V 16*, pages 647–664. Springer, 2020.
- [34] Alec Radford, Jong Wook Kim, Chris Hallacy, Aditya Ramesh, Gabriel Goh, Sandhini Agarwal, Girish Sastry, Amanda Askell, Pamela Mishkin, Jack Clark, et al. Learning transferable visual models from natural language supervision. In *International conference on machine learning*, pages 8748–8763. PmLR, 2021.
- [35] Colin Raffel, Noam Shazeer, Adam Roberts, Katherine Lee, Sharan Narang, Michael Matena, Yanqi Zhou, Wei Li, and Peter J Liu. Exploring the limits of transfer learning with a unified text-to-text transformer. *Journal of machine learning research*, 21(140):1–67, 2020.
- [36] Aditya Ramesh, Prafulla Dhariwal, Alex Nichol, Casey Chu, and Mark Chen. Hierarchical text-conditional image generation with clip latents. *arXiv preprint arXiv:2204.06125*, 1(2):3, 2022.
- [37] Aditya Ramesh, Mikhail Pavlov, Gabriel Goh, Scott Gray, Chelsea Voss, Alec Radford, Mark Chen, and Ilya Sutskever. Zero-shot text-to-image generation. In *International conference on machine learning*, pages 8821–8831. Pmlr, 2021.
- [38] Robin Rombach, Andreas Blattmann, Dominik Lorenz, Patrick Esser, and Björn Ommer. High-resolution image synthesis with latent diffusion models. In *Proceedings of the IEEE/CVF conference on computer vision and pattern recognition*, pages 10684–10695, 2022.
- [39] Chitwan Saharia, William Chan, Saurabh Saxena, Lala Li, Jay Whang, Emily L Denton, Kamyar Ghasemipour, Raphael Gontijo Lopes, Burcu Karagol Ayan, Tim Salimans, et al. Photorealistic text-to-image diffusion models with deep language understanding. *Advances in neural information processing systems*, 35:36479–36494, 2022.
- [40] Qwen Team. Qwen2.5: A party of foundation models, September 2024.
- [41] Qwen Team. Qwen2.5-vl, January 2025.

- [42] Hugo Touvron, Louis Martin, Kevin Stone, Peter Albert, Amjad Almahairi, Yasmine Babaei, Nikolay Bashlykov, Soumya Batra, Prajjwal Bhargava, Shruiti Bhosale, et al. Llama 2: Open foundation and fine-tuned chat models. *arXiv preprint arXiv:2307.09288*, 2023.
- [43] Catherine Wah, Steve Branson, Peter Welinder, Pietro Perona, and Serge Belongie. The caltech-ucsd birds-200-2011 dataset. 2011.
- [44] Ao Wang, Lihao Liu, Hui Chen, Zijia Lin, Jungong Han, and Guiguang Ding. Yoloe: Real-time seeing anything. *arXiv preprint arXiv:2503.07465*, 2025.
- [45] Olivia Wiles, Chuhan Zhang, Isabela Albuquerque, Ivana Kajić, Su Wang, Emanuele Bugliarello, Yasumasa Onoe, Pinelopi Papalampidi, Ira Ktena, Chris Knutsen, et al. Revisiting text-to-image evaluation with gecko: On metrics, prompts, and human ratings. *arXiv preprint arXiv:2404.16820*, 2024.
- [46] Jianfeng Wu, Yuting Cai, Tingyu Sun, Keer Ma, and Chunfu Lu. Integrating aigc with design: dependence, application, and evolution—a systematic literature review. *Journal of Engineering Design*, pages 1–39, 2024.
- [47] Weijia Wu, Zhuang Li, Yefei He, Mike Zheng Shou, Chunhua Shen, Lele Cheng, Yan Li, Tingting Gao, Di Zhang, and Zhongyuan Wang. Paragraph-to-image generation with information-enriched diffusion model. *arXiv preprint arXiv:2311.14284*, 2023.
- [48] Xiaoshi Wu, Yiming Hao, Keqiang Sun, Yixiong Chen, Feng Zhu, Rui Zhao, and Hongsheng Li. Human preference score v2: A solid benchmark for evaluating human preferences of text-to-image synthesis. *arXiv preprint arXiv:2306.09341*, 2023.
- [49] Qingqing Xing, Chenghong Zheng, Nan Zhu, and David Yip. Ai-generated content for academic visualization and communication in maker education. In *2023 3rd International Conference on Educational Technology (ICET)*, pages 52–56. IEEE, 2023.
- [50] Tao Xu, Pengchuan Zhang, Qiuyuan Huang, Han Zhang, Zhe Gan, Xiaolei Huang, and Xiaodong He. Attngan: Fine-grained text to image generation with attentional generative adversarial networks. In *Proceedings of the IEEE conference on computer vision and pattern recognition*, pages 1316–1324, 2018.
- [51] Peter Young, Alice Lai, Micah Hodosh, and Julia Hockenmaier. From image descriptions to visual denotations: New similarity metrics for semantic inference over event descriptions. *Transactions of the association for computational linguistics*, 2:67–78, 2014.
- [52] Jiahui Yu, Yuanzhong Xu, Jing Yu Koh, Thang Luong, Gunjan Baid, Zirui Wang, Vijay Vasudevan, Alexander Ku, Yinfei Yang, Burcu Karagol Ayan, et al. Scaling autoregressive models for content-rich text-to-image generation. *arXiv preprint arXiv:2206.10789*, 2(3):5, 2022.
- [53] Han Zhang, Tao Xu, Hongsheng Li, Shaoting Zhang, Xiaogang Wang, Xiaolei Huang, and Dimitris N Metaxas. Stackgan: Text to photo-realistic image synthesis with stacked generative adversarial networks. In *Proceedings of the IEEE international conference on computer vision*, pages 5907–5915, 2017.

Appendix

We provide more details and experiments of this work in the appendix and organize them as follows:

Appendix A, **Spatial partitioning scheme**: We present our Spatial Partitioning Scheme for categorizing bounding boxes into positional regions and validate its superior performance over the conventional nine-grid partitioning method.

Appendix B, **Configurations of evaluated models**: We detail the configurations of all evaluated models, including image resolutions and key inference hyperparameters.

Appendix C, **Time consumption and resource utilization**: We document the computational costs associated with dataset construction and model evaluation, including detailed time consumption and GPU resource utilization.

Appendix D, **Detailed human evaluation results**: We present detailed human evaluation results, validating our benchmark’s high reliability.

Appendix E, **Evaluation pipeline details**: We provide a comprehensive technical specification of our evaluation pipeline, systematically detailing the methodologies employed to assess accuracy across four critical dimensions: “Character Attributes”, “Character Locations”, “Scene Attributes”, and “Entity Relationships”.

Appendix F, **Randomness analysis for evaluation with LLMs**: We present a randomness analysis for our LLM-based evaluation pipeline, empirically confirming the reproducibility and robustness of our evaluation protocol through random seed experiments.

Appendix G, **Negative correlation between prompt length and attribute alignment**: We present the correlation analysis between prompt length and attribute accuracy in generated characters, demonstrating a consistent negative relationship between prompt length and attribute alignment fidelity.

Appendix H, **Mini DETAILMASTER Benchmark**: We introduce a mini-benchmark (800 detail-rich long prompts) that maintains evaluation consistency with the full benchmark while significantly reducing resource requirements, enabling rapid model assessment.

Appendix I, **Limitations**: We examine the limitations of our work, specifically addressing constraints in both the characteristics of our evaluation data and evaluation pipeline.

Appendix J, **Case Study**: We present representative case studies, and validate the accuracy of our comparative evaluations in the main text.

A Spatial partitioning scheme

In this section, we introduce our Spatial Partitioning Scheme, a method employed in the attribute extraction pipeline to categorize bounding boxes into approximate positional regions (e.g., “the upper part of the image”). This strategy is introduced because, in practical use, raw bounding box coordinates are typically excluded from prompts in favor of positional descriptions.

To maximize the extraction of character location features, we deviate from the conventional 3×3 grid partitioning, as we observe that characters often lie near region boundaries, making region classification difficult. Instead, we introduce slight overlaps between adjacent regions by expanding their boundaries, increasing the likelihood of larger character area coverage within a given region. This adjustment enhances the assignment of positional labels, ultimately enriching the extracted “Character Locations” features and resulting in prompts with more character location information. (Notably, this partitioning scheme is applied exclusively during attribute extraction to augment both the quantity and balance of “Character Locations” data. However, during evaluation, we do not apply this scheme and directly assess positional accuracy by comparing bounding boxes against prompt specifications using the MLLM to ensure precise measurement.)

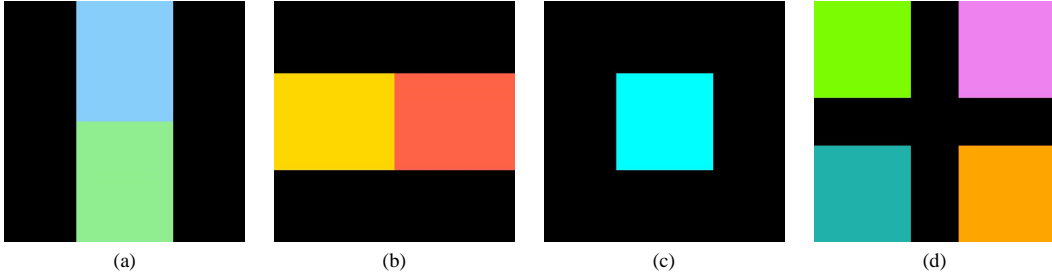


Figure 4: The visualization of the nine grids: (a) shows the upper part and the lower part; (b) shows the left part and the right part; (c) shows the middle part; while (d) shows all four corner regions: the upper left part, the lower left part, the upper right part, and the lower right part.

Our spatial partitioning scheme defines nine distinct regions within a normalized 1×1 coordinate space, where each region is represented as $[x_0, y_0, x_1, y_1]$ with (x_0, y_0) denoting the top-left coordinates and (x_1, y_1) the bottom-right coordinates. Specifically, we define: the upper part as $[0.3, 0, 0.7, 0.5]$, the lower part as $[0.3, 0.5, 0.7, 1]$, the left part as $[0, 0.3, 0.5, 0.7]$, the right part as $[0.5, 0.3, 1, 0.7]$, and the middle part as $[0.3, 0.3, 0.7, 0.7]$. Additionally, we establish four corner regions: the upper left $[0, 0, 0.4, 0.4]$, lower left $[0, 0.6, 0.4, 1]$, upper right $[0.6, 0, 1, 0.4]$, and lower right $[0.6, 0.6, 1, 1]$. As illustrated in Figure 4, this partitioning scheme provides systematic coverage of the image space while maintaining clear semantic correspondence with spatial relationships. With the nine regions, we first normalize the character’s bounding box coordinates, then calculate the proportional area overlap between the normalized box and each of the nine spatial regions. The final position classification is determined by selecting the region that covers at least 75% of the character’s bounding box area and shows the highest proportional overlap among all qualifying regions. For cases where no region meets the 75% coverage threshold (indicating boundary straddling), we assign a “null” location designation.

Table 4: Compared with the conventional 3×3 grid method, our partitioning scheme extracts richer valid character location labels and maintains matching accuracy with actual character locations.

	Proportion of “null” Character Location Labels	Matching Rate Between Labels and Actual Locations
Conventional 3×3 Grid Method	66.19%	95.91%
Our Partitioning Scheme	32.68%	95.52%

To validate the effectiveness of our nine-region partitioning scheme, we conduct a comparative analysis between the conventional 3×3 grid method and our proposed scheme by examining the proportion of ambiguous character positions (marked as “null”) at region boundaries. The experimental results show: while the traditional method classify 7,821 out of 11,816 characters (66.19%) as “null” due to boundary ambiguity, our partitioning scheme reduce this number to only 3,862 (32.68%). This reduction provides empirical evidence that our scheme effectively prevents characters from being situated near region boundaries and extracts more valid positional descriptions.

Additionally, we employ the MLLM Qwen2.5-VL-7B-Instruct to verify the consistency between our position descriptions and actual character locations, following the same method as our evaluation pipeline: we highlight characters with red bounding boxes and provide both the box coordinates and our position descriptions to the MLLM for verification. Comparative analysis reveal that while the conventional 3×3 grid method achieved 95.91% accuracy, our proposed method attain 95.52% accuracy. This marginal difference shows that our scheme successfully maintains comparable localization accuracy while significantly increasing the number of detectable character positions, confirming that our partitioning strategy achieves an optimal balance between precision and coverage.

B Configurations of evaluated models

In this section, we detail the configurations set for image generation across different models in our evaluation. Regarding the output resolution, we adopt 512×512 pixels for SD1.5 and its derivative models to align with their training settings, while setting 1024×1024 pixels for all other models. For inference steps (num_inference_steps), we follow each model’s reference implementations: 100 steps for DeepFloyd IF and ParaDiffusion, 70 steps for ELLA, and 50 steps for remaining models. The guidance scale parameters are similarly configured according to official recommendations: 11 for ELLA, 7 for DeepFloyd IF, 5 for SD-XL, 3.5 for both FLUX and SD3.5, and 7.5 for all other models.

Regarding the two proprietary models, Gemini 2.0 Flash and GPT Image-1, we access their official APIs, specifically “gemini-2.0-flash-exp-image-generation” and “gpt-image-1” respectively, setting the default hyperparameters for image generation.

For LLM Blueprint, we employ Qwen2.5-7B-Instruct as the LLM to perform attribute extraction and position extraction from long prompts. For Deepfloyd, “IF-I-XL-v1.0” serves as the first-stage model, “IF-II-L-v1.0” serves as the second-stage model, and “stable-diffusion-x4-upscaler” serves as the upscaler.

For the long-prompt optimized models, we employ the highest-performing open-source backbones available for each model. It should be noted that while superior backbones have been described in their papers, their unavailability in open-source repositories precludes their inclusion in our evaluations.

C Time consumption and resource utilization

In this section, we present the computational requirements of our data construction pipeline and evaluation pipeline.

For the first stage of our data construction pipeline (using Qwen2.5-VL-7B-Instruct and Qwen2.5-14B-Instruct), processing 164K detailed captions to produce 4,565 refined prompts on a single NVIDIA L20 GPU requires: 55 hours for “Main character identification”, 24 hours for “Character localization”, 77 hours for “Character attribute extraction”, 36 hours for “Scene attribute and entity relationship detection”, 55 hours for “Prompt refinement”, and 59 hours for “Prompt filtering”.

For the second stage of our data construction pipeline (i.e. “Prompt enhancement” with Qwen2.5-VL-72B-Instruct), processing 4,565 prompts derived from the first stage to produce 4,116 final polished prompts using 8 NVIDIA L20 GPUs requires: 3.3 hours for “Main character identification”, 6 hours

for “Character localization”, 27.4 hours for “Character attribute extraction”, 12.9 hours for “Scene attribute and entity relationship detection”, 22.6 hours for “Prompt refinement”, and 22.2 hours for “Prompt filtering”.

The evaluation pipeline typically consumes 10 hours using a single NVIDIA L20 GPU, with duration positively correlated with generated image quality.

Regarding the GPU memory, both the first stage of our data construction pipeline and the evaluation pipeline require 20GB-39GB of GPU memory. When executing the second stage of our data construction pipeline across 8 GPUs, each GPU shows memory usage ranging from 26GB to 38GB. The variation in memory requirement arises due to the different values of the “cache_max_entry_count” parameter, ranging from 0.01 to 0.8. Additionally, the previously reported time consumption is measured with the “cache_max_entry_count” parameter set to 0.8.

D Detailed human evaluation results

In this section, we provide the details of our human evaluation on **DETAILMASTER**, expanding the three metrics introduced in the main text (Task Relevance, Source Image Fidelity, and Prompt Consistency). Specifically, we systematically examine our benchmark based on the four key generation tasks.

Table 5: Human evaluation details for “Character Attributes”.

Category	Categorical Verification	Presence Confirmation	Prompt Inclusion	Attribute-Image Alignment	Attribute-Prompt Completeness
Object	100%	100%	100%	96.21%	97.64%
Animal	100%	99%	100%	98.22%	98.22%
Person	100%	98%	99%	91.58%	96.17%

For the “Character Attributes” (encompassing “object”, “animal”, and “person” categories), our annotators conduct a five-component examination for each designated main character: 1) **Categorical Verification** - determining whether the character correctly aligns with the annotated category; 2) **Presence Confirmation** - determining whether the character is in the source image; 3) **Prompt Inclusion** - determining whether the character is explicitly mentioned in the final polished prompt; 4) **Attribute-Image Alignment** - quantifying the proportion of annotated attributes that accurately align with the source image; and 5) **Attribute-Prompt Completeness** - quantifying the proportion of annotated attributes that are explicitly described in the final prompt. The results are shown in Table 5.

Table 6: Human evaluation details for “Character Locations”.

Presence Confirmation	Bounding Box Containment	Positional Accuracy	Prompt Inclusion
100%	99%	100%	99%

For the “Character Locations”, we employ a four-component spatial verification process: 1) **Presence Confirmation** - determining whether the character is in the source image; 2) **Bounding Box Containment** - determining whether the character falls in our annotated bounding box region (visually highlighted with a red rectangle); 3) **Positional Accuracy** - comparing the character’s actual placement against our position annotations (e.g., “the upper left part of the image”); and 4) **Prompt Inclusion** - checking whether the spatial information in the final prompt matches our position annotations. The results are shown in Table 6.

Table 7: Human evaluation details for “Scene Attributes”.

Category	Categorical Verification	Scene_Attribute-Image Alignment	Prompt Inclusion
Background	100%	99%	100%
Light	100%	91%	99%
Style	100%	100%	100%

For the “Scene Attributes” (covering background, lighting, and style conditions), we involve three systematic checks: 1) **Categorical Verification** - validating that the annotated “scene_attribute_content” correctly describes the annotated visual condition; 2) **Scene_Attribute-Image Alignment** - determining whether the annotated “scene_attribute_content” aligns with the source image; and 3) **Prompt**

Inclusion - determining whether the annotated “scene_attribute_content” is unambiguously specified in the final prompt. The results are shown in Table 7.

Table 8: Human evaluation details for “Entity Relationships”.

Entity_Relationship-Image Alignment	Entity_Relationship-Prompt Completeness
88.58%	97.89%

For the “Entity Relationship”, we focus on two critical aspects: (a) **Entity_Relationship-Image Alignment** - quantifying the proportion of annotated entity relationships that correctly align with the source image; and (b) **Entity_Relationship-Prompt Completeness** - quantifying the proportion of annotated entity relationships that are explicitly described in the final prompt. The results are shown in Table 8.

As shown in the human evaluation results, the evaluation data of our benchmark achieves near-perfect performance across all metrics, with most scores approaching 100%, confirming the high standard of our attribute extraction pipeline. However, a few metrics exhibit relatively lower scores, such as the Attribute-Image Alignment for the “Person” category in “Character Attributes” (91.58%), the Scene_Attribute-Image Alignment for the “Light” category in “Scene Attributes” (91%), and the Entity_Relationship-Image Alignment in “Entity Relationships” (88.58%). Notably, these metrics all pertain to the alignment between annotated features and the source images, and their failure to reach full scores suggests a few instances of hallucination during attribute extraction. Nevertheless, the corresponding “Prompt Inclusion” and “Prompt Completeness” metrics for these features consistently approach 100%, indicating that while rare discrepancies may occur between annotations and visual content, these features are still incorporated into the final prompts. This ensures that the evaluation accuracy remains largely unaffected, as the prompt-conditional generation faithfully reflects the annotated features rather than the features in the source images.

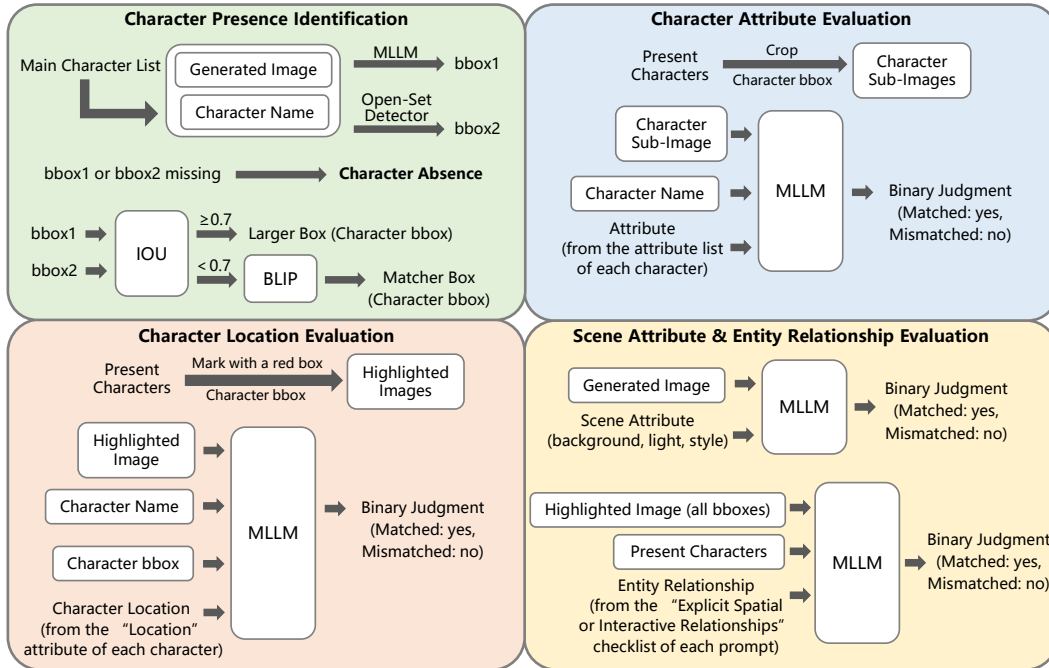


Figure 5: Overview diagram of the evaluation pipeline for the **DETAILMASTER** benchmark.

E Evaluation pipeline details

We design a multi-stage evaluation pipeline to rigorously assess compositional text-to-image generation. The pipeline initiates by instructing target text-to-image models with prompts from **DETAILMASTER** to produce corresponding image sets, followed by automated main character detection

and localization within the images. Subsequently, we perform sequential evaluations across four critical dimensions: 1) “Character Attributes”, 2) “Character Locations”, 3) “Scene Attributes”, and 4) “Entity Relationships”. This section provides comprehensive technical specifications of our evaluation pipeline, detailing the methodologies and validation mechanisms implemented for each evaluation dimension.

Character presence identification. Initially, we implement a dual-model verification system to identify which characters are successfully generated. We simultaneously employ an MLLM and the open-set detector YOLOE-11L for object detection. A character is considered successfully generated only when both models confirm its presence. For the generated characters, we further determine their locations to assist subsequent attribute evaluation. We calculate the IOU score between the two bounding boxes detected. If the score exceeds 0.7, we consider the boxes as overlapping and select the larger bounding box. Otherwise, we employ the vision-language model BLIP to compute image-text matching scores between both bounding box regions and the character name, selecting the box with the higher score. Identifying character presence can accelerate the whole evaluation process by eliminating redundant computations for failed generations. And it also avoids repetitive detection steps as the positional information can be reused.

“Character Attribute” evaluation. For character attribute evaluation, we sequentially process each identified character and extract sub-images based on their positional information. Subsequently, we employ an MLLM to evaluate every attribute in the pre-built attribute list for each character. The MLLM provides binary judgments (“yes” or “no”) for each attribute based on the sub-image content. We then quantify the number of correctly generated attributes. Finally, the character attribute accuracy is calculated separately across three distinct categories: objects, animals, and persons, to enable category-specific performance analysis.

“Character Location” evaluation. For character location evaluation, we sequentially process each identified character and mark its position in the generated image with a red bounding box. The bounding box information is then provided to the MLLM along with explicit instructions that the red box marks the target character. And the MLLM is prompted to determine whether the character precisely aligns with the position specified in its “Character Location” attribute, responding with a yes/no judgment. The final character location accuracy is calculated as the proportion of correctly positioned characters to the total number of characters who have “Character Location” attribute.

“Scene Attribute” evaluation & “Entity Relationship” evaluation. For scene attribute evaluation, we simply ask the MLLM to determine whether the generated images satisfy each specified “Scene Attribute” with yes/no responses. The accuracy rates are calculated separately for background, lighting, and style attributes. Regarding entity relationship evaluation, for each generated image, we first mark all identified characters in the image with red bounding boxes. We then provide the MLLM with the marked image and the list of identified characters, and subsequently ask it to evaluate each attribute in the “Explicit Spatial/Interactive Relationships” checklist, determining whether the specified entity relationship aligns with the image content.

F Randomness analysis for evaluation with LLMs

To assess the impact of randomness inherent in LLM-based evaluation, we conduct experiments by varying random seeds and setting the LLM temperature to 0.8, subsequently repeating evaluation across five representative models (SD1.5, LongAlign, LLM Blueprint, FLUX.1-dev, and GPT Image-1) to quantify stochastic variability. The results are shown in 9.

The presented results show that the randomness introduced by LLMs in our evaluation framework has minimal impact, with repeated assessments across all models showing negligible variations ($\Delta < 0.5\%$). This robust consistency strongly validates the stability and reliability of our evaluation protocol, ensuring reproducible and dependable model comparisons regardless of inherent LLM randomization factors.

Table 9: Robustness evaluation of LLM-based assessment randomness.

Model	Character Attributes			Character Locations	Scene Attributes			Spatial Attributes
	Object	Animal	Person		Background	Light	Style	
FLUX.1-dev (1)	51.47	45.83	34.91	41.57	95.77	97.05	94.81	47.49
FLUX.1-dev (2)	51.72	45.89	35.60	41.57	95.77	97.05	94.81	47.49
FLUX.1-dev (3)	51.53	45.85	34.97	41.57	95.77	97.05	94.81	47.45
GPT Image-1 (1)	59.47	48.12	40.43	53.93	97.50	98.85	97.69	63.03
GPT Image-1 (2)	59.47	48.12	40.43	53.93	97.50	98.85	97.69	63.03
GPT Image-1 (3)	59.47	48.12	40.43	53.93	97.50	98.85	97.69	63.03
LLM Blueprint (1)	21.41	27.01	13.91	18.44	50.89	77.57	64.24	11.60
LLM Blueprint (2)	21.42	26.97	13.85	18.46	50.89	77.57	64.24	11.65
LLM Blueprint (3)	21.32	26.97	13.67	18.46	50.89	77.57	64.24	11.62
LongAlign (1)	32.95	34.60	15.35	14.89	77.03	87.70	72.27	19.17
LongAlign (2)	32.95	34.60	15.35	14.89	77.03	87.70	72.27	19.09
LongAlign (3)	32.99	34.56	15.38	14.92	77.03	87.70	72.27	19.11
SD1.5 (1)	20.79	27.69	13.89	8.68	22.02	64.52	80.90	5.88
SD1.5 (2)	20.76	27.68	13.92	8.68	22.02	64.52	80.90	5.84
SD1.5 (3)	20.78	27.62	13.93	8.68	22.02	64.52	80.90	5.84

G Negative correlation between prompt length and attribute alignment

In this section, we analyze the relationship between prompt length and attribute accuracy for detected generated characters (categorized into objects, animals, and persons) to examine how the model’s attribute adherence capability and resistance to attribute misalignment vary with increasing prompt length. As illustrated in Figure 6, the left, middle, and right subgraph respectively show the attribute accuracy trends for “object”, “animal”, and “person” characters.

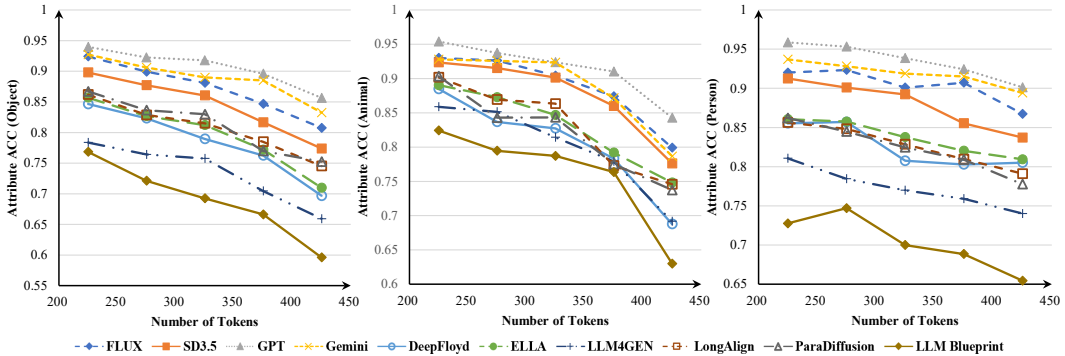


Figure 6: Negative correlation between prompt length and attribute alignment.

The trends show a clear inverse correlation between prompt length and attribute accuracy, indicating that longer prompts lead to progressively greater deviations from the intended character descriptions, manifested as attribute misalignment and omission. Notably, the performance comparison reveals that models specifically trained with long prompts (e.g., ELLA and ParaDiffusion) exhibit more gradual accuracy degradation compared to models using conventional training like Deepfloyd, as evidenced by their shallower accuracy decline curves. These findings collectively suggest that current text-to-image generation systems still face substantial challenges in maintaining attribute consistency with long prompts, highlighting the critical need for further research into long-prompt optimization techniques and training methodologies to advance this crucial capability.

H Mini DETAILMASTER Benchmark

To address computational resource constraints and facilitate rapid evaluation for researchers, we develop a mini version of our **DETAILMASTER** benchmark comprising 800 detail-rich long prompts. The construction methodology for the mini benchmark employs a sampling approach across four key dimensions: 1) For “Character Attributes”, we analyze the distribution of object, animal, and person

entities in each sample, selecting candidates containing more than two instances of each category into respective attribute candidate pools (i.e., “Object Attributes”, “Animal Attributes”, “Person Attributes”); 2) For “Character Locations”, samples featuring more than three localizable characters are included in the location candidate pool; 3) For “Scene Attributes”, candidates are selected based on the presence of background descriptions, lighting conditions, or style specifications (i.e., “Background Attributes”, “Lighting Attributes”, “Style Attributes”); 4) For “Entity Relationships”, samples are filtered by requiring a minimum of five spatial or interactive relationships. The final mini benchmark composition is achieved through balanced random sampling, extracting 100 prompts from each of these eight candidate pools to form a representative yet efficient evaluation set. We conduct a comprehensive reevaluation of all 12 models discussed in the main text using our mini **DETAILMASTER** benchmark, with the comparative results presented in Table 10.

Table 10: Evaluation results on the **mini DETAILMASTER** Benchmark. All values in the table represent accuracy percentages.

(A) General-Purpose Text-to-Image Model									
Model	Backbone	Character Attributes			Character Locations	Scene Attributes			Spatial Attributes
		Object	Animal	Person		Background	Light	Style	
SD1.5	-	14.76	21.81	9.85	7.11	20.11	65.62	85.94	6.03
SD-XL	-	18.48	21.92	11.58	10.87	26.36	69.01	70.05	8.22
DeepFloyd	-	22.40	23.85	20.77	14.72	24.52	68.23	86.98	12.60
SD3.5 Large	-	36.36	32.27	23.00	35.45	94.57	88.80	98.70	35.99
FLUX.1-dev	-	37.90	38.57	27.43	46.66	97.83	97.14	95.83	43.04
Gemini 2.0 Flash	-	47.21	36.82	27.14	46.15	97.67	96.88	98.91	46.35
GPT Image-1	-	50.96	39.42	31.23	66.06	98.75	98.84	95.40	55.87

(B) Long-Prompt Optimized Text-to-Image Model									
Model	Backbone	Character Attributes			Character Locations	Scene Attributes			Spatial Attributes
		Object	Animal	Person		Background	Light	Style	
LLM4GEN	SD1.5	16.47	23.84	15.48	7.53	23.64	67.71	51.56	6.30
LLM Blueprint	SD1.5	15.57	23.51	14.29	17.93	54.46	76.67	53.03	10.40
ELLA	SD1.5	28.09	24.96	16.64	14.46	51.36	68.75	36.20	12.13
LongAlign	SD1.5	26.08	23.42	13.91	15.97	85.60	81.25	63.80	15.45
ParaDiffusion	SDXL	28.97	28.40	17.51	18.56	89.40	88.80	60.36	18.66

The comparative results in Table 10 show that the performance comparison and trends across models remain consistent between our mini **DETAILMASTER** benchmark and the full **DETAILMASTER** benchmark. As the mini benchmark contains more challenging samples selected for their greater detail complexity, the scores on the mini benchmark are generally lower than those on the full version. Crucially, the preserved consistency combined with improved evaluation efficiency enables researchers to more effectively assess model performance in handling long prompts. Therefore, the mini benchmark serves as an efficient alternative for resource-constrained scenarios or time-sensitive evaluations, while maintaining comparable validity to the full benchmark.

I Limitations

Regarding the quality of our benchmark data, we have conducted systematic sampling assessments involving professional annotators, validating the high quality of our dataset, with detailed results presented in Appendix D. Section 5.1 further shows the substantial scale and diversity of our evaluation data, while Table 1 provides comparative analyses highlighting its superior suitability for long-prompt scenarios relative to existing benchmarks. However, our current metrics, while extending T2I-CompBench’s metrics with “Character Locations” and “Scene Attributes”, remain potentially expandable through other dimensions such as aesthetic assessment or human preference scoring. Furthermore, the current prompt collection primarily focuses on realistic imagery and user-uploaded photographs, with limited representation of artistic works. Future work could develop a dedicated subset to evaluate artistic content generation.

Regarding our evaluation protocol, while it leverages LLMs as its core evaluation mechanism, with robustness verified in Appendix F where we demonstrate minimal impact of model randomness on evaluation outcomes, it presents notable computational demands. The current implementation requires substantial GPU resources (minimum 20GB VRAM) and exhibits longer processing times compared to conventional evaluation methods. These resource-intensive characteristics may limit

accessibility for some research teams. To address these constraints, we will investigate alternative evaluation methods that can maintain assessment accuracy while improving computational efficiency.

J Case studies

'polished_prompt': "A high angle shot of a brown wooden bench with several dishes on top of it. In the center and on the left are two round, wavy side plates with black scratches on the sides and a doily pattern engraved on the plates. On both plates is a thick brown cookie that's been crosscut at the top, located in the middle part of the image. The plate on the right has a candy with a yellow wrapper and green ends. To the right of the plates is a white mug with whipped cream on top that is similar to the glass plates. The cup, made of ceramic material, has a cylindrical shape with a handle and a textured surface. The white whipped cream on top is frothy and has an embossed design. Surrounding the wooden bench is a dark brown wooden floor. On the top right is a gray curtain, and on the upper left is a view of the lower part of a white wooden wall. The image is taken indoors with soft, warm lighting, likely from an overhead source, creating a cozy and inviting atmosphere. The lighting is evenly distributed, with no harsh shadows, suggesting a relaxed time of day, possibly evening. The style of the image is a realistic photo with a warm, homely aesthetic. The brown wooden bench supports the two round, wavy side plates with black scratches and a doily pattern, which are placed side by side. The thick brown cookies crosscut at the top are positioned on top of the two round, wavy side plates, with one cookie on each plate. The candy with a yellow wrapper and green ends is located on the right plate, next to the thick brown cookie. The white mug with whipped cream on top is situated to the right of the two round, wavy side plates. The two round, wavy side plates are adjacent to each other, with the plate containing the candy being closer to the white mug with whipped cream on top."

'character_attributes': [{'main_character': 'brown wooden bench', 'characteristics_list': ['several dishes on top'], 'cls': 'object'}, {'main_character': 'two round, wavy side plates with black scratches and a doily pattern', 'characteristics_list': ['two round, wavy side plates', 'black scratches on the sides', 'doily pattern engraved on the plates'], 'cls': 'object'}, {'main_character': 'thick brown cookies crosscut at the top', 'characteristics_list': ['thick brown cookie that's been crosscut at the top', 'thick brown cookie'], 'cls': 'object'}, {'main_character': 'white mug with whipped cream on top', 'characteristics_list': ['white mug', 'whipped cream', 'ceramic material', 'cylindrical shape', 'handle', 'textured surface', 'frothy topping', 'embossed design'], 'cls': 'object'}]

'character_locations': [{'main_character': 'thick brown cookies crosscut at the top', 'bbox': [765, 740, 1098, 996], 'position': 'The middle part of the image'}]

'scene_attributes': [{'scene_attribute': 'background', 'content': 'The background features a dark brown wooden floor and a white wooden wall with a gray curtain on the right side.'}, {'scene_attribute': 'light', 'content': 'The image is taken indoors with soft, warm lighting, likely from an overhead source, creating a cozy and inviting atmosphere. The lighting is evenly distributed, with no harsh shadows, suggesting a relaxed time of day, possibly evening.'}, {'scene_attribute': 'style', 'content': 'The style of the image is a realistic photo with a warm, homely aesthetic.'}, {'scene_attribute': 'spatial', 'content': 'The brown wooden bench supports the two round, wavy side plates with black scratches and a doily pattern, which are placed side by side.', 'The thick brown cookies crosscut at the top are positioned on top of the two round, wavy side plates, with one cookie on each plate.', 'The candy with a yellow wrapper and green ends is located on the right plate, next to the thick brown cookie.', 'The white mug with whipped cream on top is situated to the right of the two round, wavy side plates.', 'The two round, wavy side plates are adjacent to each other, with the plate containing the candy being closer to the white mug with whipped cream on top.'}]

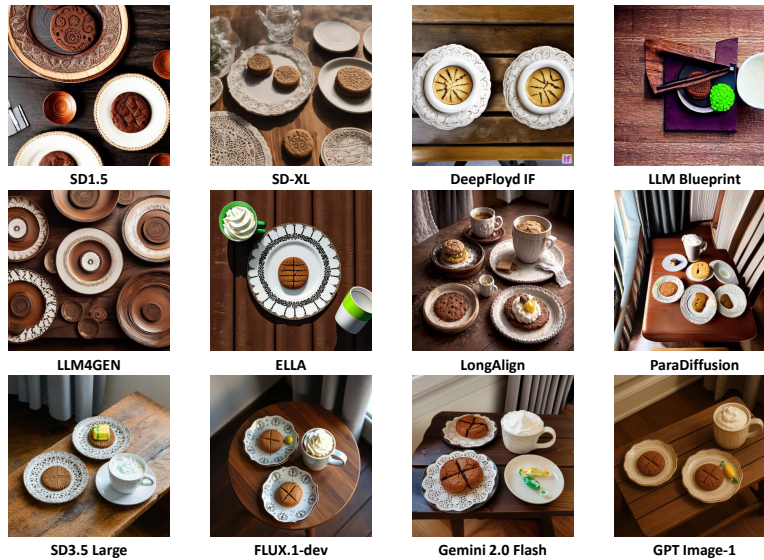


Figure 7: Comparative visualization set for case study 1.

The first challenging case study reveals that long-prompt optimized models exhibit superior completeness in main character generation compared to their backbone counterparts, with the four most advanced models achieving the highest fidelity. Regarding fine-grained details such as “crosscut at the top”, “cookies in the middle”, and “a gray curtain on the right side”, only the four most advanced models adhere to the instructions, with some remaining inaccuracies and omissions. While long-prompt optimized models (e.g., ParaDiffusion) interpret such details from the input, their generative capability remains constrained by backbone limitations, as evidenced by partial failures (e.g., generating cookies but omitting the crosscut).

'polished_prompt': 'A medium-close-up view of a small shed that is made up of light brown wooden planks that run vertically, and along these planks there are two rectangular openings that are round along the top. Inside the windows, there are brown wooden planks that run vertically. In between these openings there is a blue banner that has two drawings of an owl and a woman to the left who is facing the owl, and the owl is standing on the woman's arm. To the left of the window, there is another banner that is light blue, and along it there is black text that reads "WILDLIFE REVE" vertically. The roof of the shed is triangular and gray and is being lit up by the sun, with the light source positioned to the front-left, casting soft shadows on the shed. In the upper part of the image, in front of the roof, there is a small falcon that is flying across and to the left, with its sharp beak, outstretched wings, streamlined body, and feathered tail, showcasing its natural predator instincts and agile flight. The falcon is positioned above the light blue banner with black text "WILDLIFE REVE". Behind the shed is a tall tree that has a little bit of green foliage along it, and to the right of the tree are multiple trees that have no leaves along them. Behind the trees, a clear blue sky is visible, indicating a daytime setting in a natural or semi-natural environment. The image is brightly lit with natural sunlight, suggesting the light intensity is high, typical of midday. The style of the image is a realistic photo. It is daytime.'

'character_attributes': [{'main_character': 'small shed with light brown wooden planks and two arched openings', 'characteristics_list': ['made up of light brown wooden planks', 'planks that run vertically', 'two rectangular openings that are round along the top', 'brown wooden planks that run vertically inside the windows', 'triangular and gray roof', 'roof being lit up by the sun'], 'cls': 'object'}, {'main_character': 'blue banner with drawings of an owl and a woman', 'characteristics_list': ['blue banner', 'two drawings of an owl', 'woman to the left', 'facing the owl', "owl is standing on the woman's arm"], 'cls': 'object'}, {'main_character': 'light blue banner with black text "WILDLIFE REVE"', 'characteristics_list': ['light blue banner', 'black text', 'WILDLIFE REVE'], 'cls': 'object'}, {'main_character': 'small falcon flying in front of the shed', 'characteristics_list': ['animal', 'small falcon', 'flying', 'sharp beak', 'outstretched wings', 'streamlined body', 'in motion', 'feathered tail', 'agile flight'], 'cls': 'animal'}]

'character_locations': [{'main_character': 'small falcon flying in front of the shed', 'bbox': [674, 515, 906, 730], 'position': 'The upper part of the image'}]

'scene_attributes': [{'scene_attribute': 'background', 'content': 'The background features a clear blue sky and a mix of trees, some with green foliage and others bare, indicating a daytime setting in a natural or semi-natural environment.'}, {'scene_attribute': 'light', 'content': 'The image is brightly lit with natural sunlight, indicating a daytime setting, and the light source is positioned to the front-left, casting soft shadows on the shed. The clear blue sky suggests the light intensity is high, typical of midday.'}, {'scene_attribute': 'style', 'content': 'The style of the image is a realistic photo.'}, {'scene_attribute': 'spatial', 'content': ["The small falcon flying in front of the shed is positioned above the light blue banner with black text 'WILDLIFE REVE'.", "The blue banner with drawings of an owl and a woman is located between the two arched openings of the small shed with light brown wooden planks.", "The light blue banner with black text 'WILDLIFE REVE' is to the left of the blue banner with drawings of an owl and a woman.", "The small shed with light brown wooden planks and two arched openings is situated behind the small falcon that is flying in front of it."]}]



Figure 8: Comparative visualization set for case study 2.

The second challenging case study reveals systematic limitations across model categories: 1) Outdated models without long-prompt optimization fail to generate numerous specified characters, demonstrating catastrophic prompt adherence failures. 2) Long-prompt optimized models show improved yet incomplete character generation, indicating persistent architectural constraints. 3) Advanced models show critical shortcomings in detail fidelity. SD3.5 and FLUX fail to render the specified “blue banner with drawings of an owl and a woman”, while Gemini 2.0 Flash and GPT Image-1 produce inaccurate textual elements (“WILDLIFE REVE”). These findings collectively underscore the ongoing challenges in compositional reasoning and detail preservation across current T2I models in long prompt scenarios.